ACS APPLIED MATERIALS & INTERFACES

Research Article

www.acsami.org

Nitrogen-Doped Graphene for Generation and Evolution of Reactive Radicals by Metal-Free Catalysis

Xiaoguang Duan,[†] Zhimin Ao,[‡] Hongqi Sun,*[,†] Stacey Indrawirawan,[†] Yuxian Wang,[†] Jian Kang,[†] Fengli Liang,[§] Z.H. Zhu,[§] and Shaobin Wang*[,†]

[†]Department of Chemical Engineering, Curtin University, GPO Box U1987, Bentley, Western Australia 6845, Australia

[‡]Centre for Clean Energy Technology, School of Chemistry and Forensic Science, University of Technology, Sydney, PO Box 123, Sydney, New South Wales 2007, Australia

[§]School of Chemical Engineering, The University of Queensland, St Lucia, Queensland 4072, Australia

Supporting Information

ABSTRACT: N-Doped graphene (NG) nanomaterials were synthesized by directly annealing graphene oxide (GO) with a novel nitrogen precursor of melamine. A high N-doping level, 8−11 at. %, was achieved at a moderate temperature. The sample of NG-700, obtained at a calcination temperature of 700 °C, showed the highest efficiency in degradation of phenol solutions by metal-free catalytic activation of peroxymonosulfate (PMS). The catalytic activity of the N-doped rGO (NG-700) was about 80 times higher than that of undoped rGO in phenol degradation. Moreover, the activity of NG-700 was 18.5 times higher than that of the most popular metal-based catalyst of nanocrystalline Co_3O_4 in PMS activation. Theoretical calculations using spin−unrestricted density functional theory (DFT) were carried out to probe the active sites for PMS activation on N-doped graphene. In addition, experimental detection of generated radicals using electron paramagnetic resonance (EPR) and competitive radical reactions was performed to reveal the PMS activation processes and pathways of phenol degradation on nanocarbons. It was observed that both $^{\bullet}OH$ and $SO_4^{\bullet-}$ existed in the oxidation processes and played critical roles for phenol oxidation.

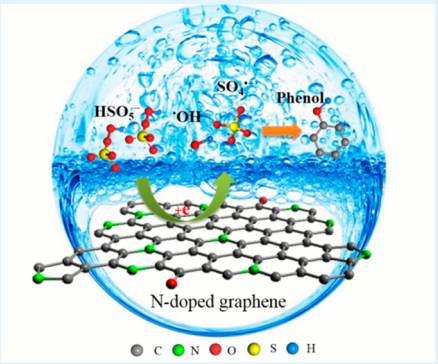

KEYWORDS: *nitrogen doping, graphene, peroxymonosulfate, phenol degradation, metal-free catalysis, DFT*

1. INTRODUCTION

In the past two decades, nanocarbons such as carbon nanotubes (CNTs), graphene oxide (GO), reduced graphene oxide (rGO), graphene, graphitic carbon nitride (g-C_3N_4), and other graphene-like materials have attracted worldwide attention, owing to the large theoretical surface area, high thermal conductivity, unique electronic property, and sp^2-hybridized carbon configuration.[1−3] Studies on metal-free catalysis have demonstrated that nanocarbons can play promising roles in various catalytic processes for energy and environmental applications.[4−6] The employment of nanocarbons in water treatment as an alternative to metal-based catalysts, such as Co, Fe or Mn, is expected to completely avoid metal leaching and the associated secondary contamination. However, current applications of metal-free catalysis are mainly for energy and chemical synthesis,[7,8] and metal-free remediation has been less explored.

As one of advanced oxidation processes (AOPs), catalytic oxidation by sulfate radicals ($SO_4^{\bullet-}$) from peroxymonosulfate (PMS) has been applied to decompose the hazardous organic compounds in wastewater. Compared to hydroxyl radicals ($^{\bullet}OH$) in Fenton reaction, $SO_4^{\bullet-}$ demonstrated a higher oxidative potential (2.5−3.1 V vs 2.7 V of $^{\bullet}OH$), and can adapt to a wide pH range.[9] Homogeneous Co(II)/PMS and Mn(II)/PMS systems have been proven to be highly effective to generate active radicals for the AOPs.[9,10] Nevertheless, the loss of toxic metals leads to severe environmental issues, giving rise to high risks to human beings. Heterogeneous catalysis using cobalt oxides,[11] supported cobalt oxides,[12] or manganese oxides[13] has been investigated, yet leaching is still inevitable. Therefore, novel metal-free catalysts with high catalytic efficiency are urgently required in terms of green catalysis for wastewater remediation.

In pioneering studies, we found that rGO prepared by a hydrothermal method can effectively promote PMS activation to generate active radicals for degradation of phenol, chlorophenols, and dyes in aqueous solution.[14] It was also found that the zigzag edges and ketonic groups (C═O) on the edges of graphene might be the active sites for PMS activation. The delocalized electrons at the zigzag edges and little amount of oxygen-containing groups with rich electrons can present a great potential for the redox process.[15,16] To improve the catalytic performance, structural modification was carried out by physical and/or chemical activation of rGO.[17,18] The specific

Received: December 1, 2014
Accepted: January 29, 2015
Published: January 29, 2015

DOI: 10.1021/am508416n
ACS Appl. Mater. Interfaces 2015, 7, 4169−4178

Scheme 1. Synthesis Procedure of N-Doped Graphene

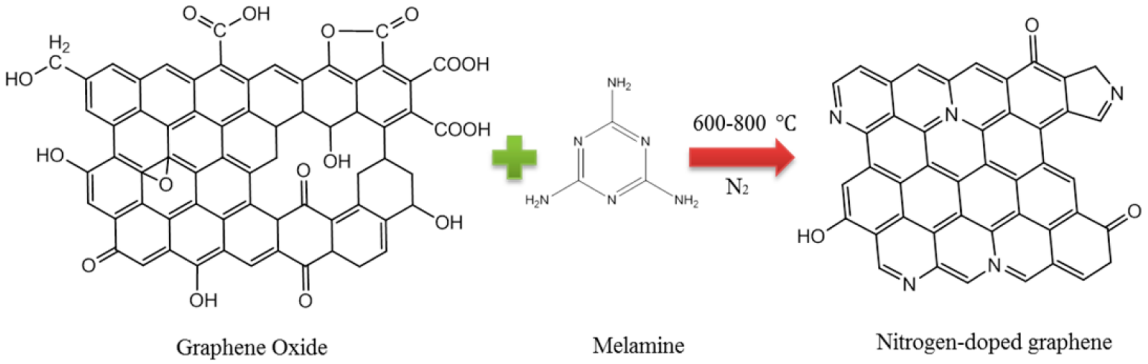

surface area (SSA) of rGO can be increased from 200 to 1200 m^2/g and the activated porous rGO demonstrated to be highly effective for adsorptive and oxidative removal of phenol and methylene blue (MB) in water. The studies also suggested that both oxygen groups and SSA played key roles in adsorption and catalytic oxidation of MB.[17]

It was expected that chemical compositional modification would bring out instinct changes to nanocarbons, more significant than structural modification. It has been reported that doping heteroatoms (e.g., N, B, and P) into the carbon honeycomb network can create more active sites and bring new properties such as increasing the electrochemical catalytic activity, hydrophilicity, and higher selectivity toward oxidative dehydrogenation (ODH) reaction and oxygen reduction reaction (ORR).[16,19] In environmental remediation, we proved that modification of rGO and pristine multiwalled carbon nanotubes (MWCNTs) with nitrogen atoms using ammonium nitrate as the N precursor can dramatically boost the performance of PMS activation.[20,21] The SSA of N-rGO-350 was found to be as low as 64.1 m^2/g, and the nitrogen doping level was 5.61 at. %.

In this study, we presented a simple thermal process for synthesis of rGO with both structural and compositional modification. The prepared N-doped graphene (NG) presented a larger SSA (227.5 m^2/g) and a higher N-doping level (9.68 at. %). A stunning 80-fold enhancement was achieved on NG-700 in catalytic oxidation of phenol solutions compared with unmodified rGO. N-doped rGO also showed superior performance to g-C_3N_4, graphene nanosheets (GNs), rGO, single-walled carbon nanotube (SWCNT), N-doped graphene and carbon nanotube N-doped graphene and carbon nanotube utilizing ammonium nitrate as nitrogen precursors, and a typical metal-based catalyst of crystalline Co_3O_4. Computational studies, electron paramagnetic resonance (EPR) spectra and competitive radical reactions facilitated the first insights into the mechanism of PMS activation by the nanocarbons and the evolution of sulfate radicals in phenol oxidation.

2. EXPERIMENTAL SECTION

2.1. Materials and Chemicals. Graphite powder (purity 99.9995%), potassium permanganate ($KMnO_4$), sulfuric acid (95–97%), and potassium peroxymonosulfate ($2KHSO_5{\cdot}3KHSO_4{\cdot}K_2SO_4$, Oxone) were purchased from Sigma-Aldrich. Hydrogen peroxide (30%, H_2O_2) was obtained from Chem-Supply. Phenol was obtained from Ajax Finechem. 5,5-Dimethyl-1-pyrroline (DMPO, >99.0%) was obtained from Fluka. The multiwalled carbon nanotubes (MWCNTs), single-walled carbon nanotubes (SWCNTs), and graphene nanosheets (GNs) were purchased from Chengdu Organic Chemical, China. All chemicals were used as received without further purification.

2.2. Synthesis of Nitrogen-Doped Graphene. Graphite oxide (GO) was synthesized through a modified Hummers' method (detailed procedure shown in the Supporting Information)[22] and used for preparation of N-doped rGO. The preparation procedure is shown in Scheme 1. In a typical synthesis, GO (1.0 g) was dissolved in 50 mL of ethanol, stirred for 30 min, and sonicated for another 30 min. Then melamine (1.0 g) was added to the mixed solution, and then the suspension was heated to 50 °C on a hotplate to evaporate the ethanol gradually while stirring. The dried mixture was first heated in a muffle furnace at 450 °C and then in a tubular furnace for further calcination at 600, 700, and 800 °C for 1 h under N_2 atmosphere to obtain NG-600, -700, and -800, respectively. The samples were washed with ultrapure water and ethanol for several times and dried in an oven at 60 °C overnight. Thus, the nitrogen-doped graphene (NG) was obtained.

2.3. Characterization of Materials. X-ray diffraction (XRD) patterns were acquired on a D8-Advanced diffractometer system from Bruker with Cu Kα radiation (λ = 1.5418 Å). Fourier transform infrared spectra (FTIR) were obtained from a Bruker instrument with ATR correction mode. Thermogravimetric-differential thermal analysis (TG-DTA) was recorded on a PerkinElmer Diamond thermal analyzer with a heating rate of 10 °C/min in air. The Brunauer–Emmett–Teller (BET) equation and Barrett–Joyner–Halenda (BJH) method were utilized to evaluate the specific surface area and pore size distribution of the carbon materials, respectively. Total organic carbon (TOC) was measured on a Shimadzu TOC-vcph analyzer. Raman spectra were obtained by using an ISA argon-laser Raman spectrometer. X-ray photoelectron microscopy (XPS) was conducted on a Thermo Escalab 250 using an Al Kα X-ray source to detect the elemental composition of carbon materials. The morphological information was analyzed on a Zeiss Neon 40EsV FIBSEM by scanning electron microscopy (SEM) images. Electron paramagnetic resonance (EPR) from a Bruker EMS-plus was applied to probe the reactive radicals generated during activation of PMS captured by a spin trapping agent 5,5-dimethylpyrroline-oxide (DMPO), operating with center field of 3515G, sweep width of 100G, microwave frequency of 9.86 GHz, power setting of 18.75 mW, and scan number of 3. The EPR spectra were analyzed by the spin-fitting package of Bruker Xeon software.

2.4. Evaluation of Phenol Catalytic Oxidation. The catalytic oxidation of phenol was performed in a 250 mL conical flask with phenol solution (20 ppm), catalyst (0.1 g/L), and PMS (2 g/L) in a constant temperature controlled water bath for the kinetic study. During each time interval, 1 mL of solution was withdrawn by a syringe, filtered by a 0.45 μm Millipore film, and injected into a vial. Then 0.5 mL of methanol was also injected into the reaction solution as a quenching reagent. The mixed solution was analyzed by a high performance liquid chromatography (HPLC, Varian). The organics were separated by a C-18 column and analyzed by a UV detector (270 nm). The mobile phase was made of 30% acetonitrile and 70% ultrapure water and at a flow rate of 1 mL/min. The intermediates tests were carried out with a flow rate of 0.1 mL/min at 220 nm.

DOI: 10.1021/am508416n
ACS Appl. Mater. Interfaces 2015, 7, 4169–4178

Scheme 2. Atomic Structures of Graphene before and after N-Doping[a]

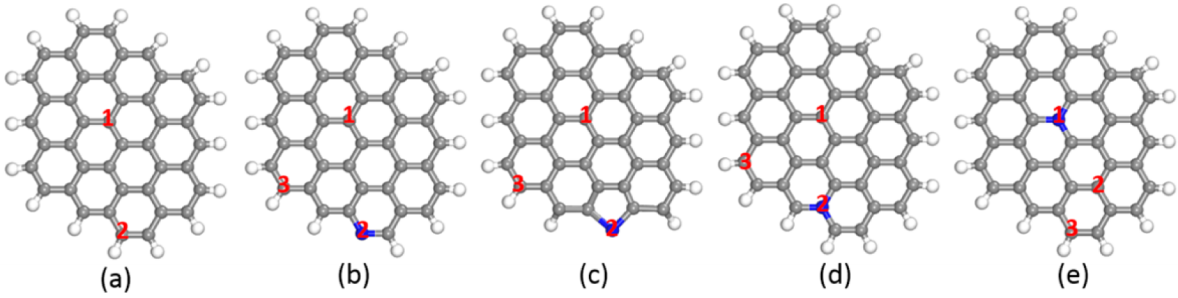

[a]Pristine graphene (a) and graphene with different doping types ((b) pyridinic N, (c) pyrrolic N, and (d, e) graphitic N) are considered. The numbers indicate the adsorption sites of the H atom we considered. In this figure, the gray, white, and blue balls are C, H, and N atoms, respectively.

2.5. Computational Models and Methodology. The spin−unrestricted density functional theory (DFT) calculations were carried out using Dmol^3 package.[23] Exchange−correlation functions were taken as generalized gradient approximation (GGA) with Perdew−Burke−Ernzerhof (PBE).[24] Double numerical plus polarization (DNP) was employed as the basis set. The convergence tolerance of energy of 10^{-5} Hartree was applied (1 Hartree = 27.21 eV), and the maximal allowed force and displacement were 0.002 Hartree/Å and 0.005 Å, respectively. In the simulation, nonperiodic graphene cluster was employed in the calculation, as shown in Scheme 2 below. The DFT+D method within the Grimme scheme[25] was used in all calculations to take the van der Waals forces into account.

3. RESULTS AND DISCUSSION

3.1. Characterization of Carbon Materials. XRD patterns of GO and nitrogen doped rGO samples are shown in Figure 1. The strong peak at 2θ = 10.2° is corresponding to

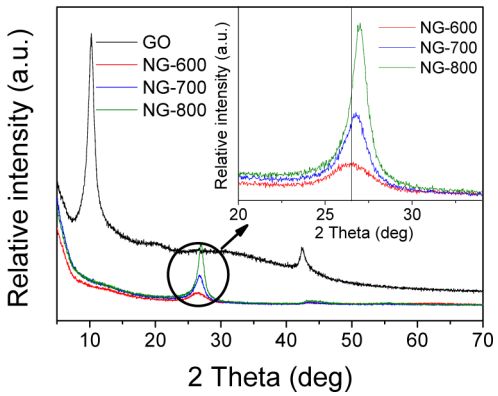

Figure 1. XRD patterns of GO and N-doped rGO. Inset: high-resolution of graphite phase.

the graphene oxide (002) reflection, demonstrating that a well-ordered and layered structure of GO is formed. The interlayer space (0.86 nm) is larger than that of pristine graphite (0.34 nm), indicating that the oxygen groups were introduced into the graphitic layer and the C═C double bonds were formed. After reduction, the peak at 2θ = 10.2° disappeared and a small sharp peak at 2θ = 25.1° emerged. The XRD patterns also showed that the degree of crystallinity (peak intensity) of the nitrogen-doped graphene increased with elevated temperature, while the peak was shifted to a higher 2θ degree, implying a better reducibility owing to removal of surface functional groups and that nitrogen atoms were successfully doped into the graphitic system.[26]

Figure 2 presents SEM images of GO, rGO-700, and NG-700. It can be seen that exfoliated layers were found in rGO-700 and NG-700. Compared with the silk veil-like morphology of rGO-700, partially aggregated and crinkled structure was obtained at the end of doped graphene sheets, originated from the created defective sites after nitrogen atoms incorporated into the graphene layer. It was reported that the GO layers would be refabricated when they were annealed at a high temperature and can be influenced by the heteroatom doping process.[27]

Raman spectra have been widely used to investigate the degree of graphitization, number of layers, and doping status of graphene.[28] Figure 3 displays the Raman spectra of GO, rGO-700, and NG-700. The integrated intensity ratio of D band versus G band (I_D/I_G) is a significant parameter to reflect the defect and disorder level in the graphitic carbon layers.[29] The I_D/I_G value of NG-700 (1.34) is higher than those of GO (1.22) and rGO-700 (1.28), indicating that more defective sites were created through the incorporation of nitrogen atoms into the carbon network. The strong D band indicated that the N-doping would significantly enhance the defect density. It was reported that width of G band would be changed when doping with heteroatoms.[30,31] In this study, the G bandwidth came along with the order as NG-700 > GO > rGO-700, suggesting that N atoms were doped into the sp^2 carbon networks.

Figure 4 shows nitrogen sorption isotherm, pore size distribution and BET surface area of three NG samples doped at varying temperatures. It can be been seen that NG-700 has a higher surface area (227.5 m^2/g) than NG-600 (64.4 m^2/g) and NG-800 (104.9 m^2/g). For carbon materials, high annealing temperature usually brings about porous structure, smaller nanocrytalline graphene sheets, and larger surface area, hereby creating more edges and defects.[17] However, the decreased surface area for NG-800 may be ascribed to the collapse of the carbon skeleton structure when the temperature is over 700 °C. Figure 4b indicates that the pore structures of the NG catalysts prepared are primarily consisted of micro- and mesopores (0−5 nm).

Figure 5 displays XPS survey (0−1000 eV) of N-doped graphene to explore the chemical compositions. Figure 5a shows that the oxygen levels of NG-600, -700, and -800 were measured to be 3.28, 3.11, and 2.41%, respectively, which were much lower than that of GO with an oxygen level of 45%.[32] The oxygen-containing groups in GO and their changes upon reduction and nitrogen doping are shown in Figure S1 (Supporting Information). It has been reported that the acid oxygen groups like carboxyl and lactone began to decompose into CO_2 at about 250 °C, and the neutral and weak basic

DOI: 10.1021/am508416n
ACS Appl. Mater. Interfaces 2015, 7, 4169−4178

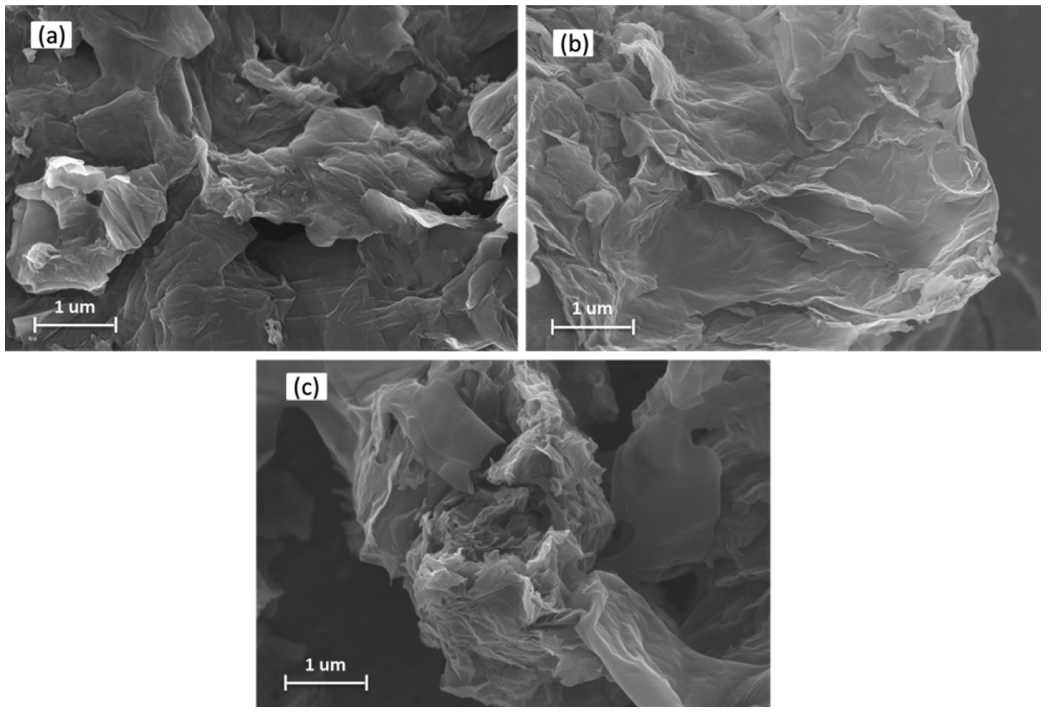

Figure 2. SEM images of GO (a), rGO-700 (b), and NG-700 (c).

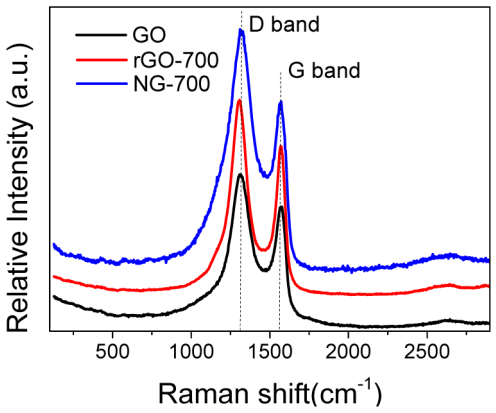

Figure 3. Raman spectra of GO, rGO-700, and NG-700.

surface groups such as epoxide, quinone, phenol, and carbonyl would be volatilized into CO and CO_2 between 450 and 900 °C.[33,34] The desorption and decomposition properties of GO, NGs, and the N precursor (melamine) are shown in Figure S2 (Supporting Information). Previous research also revealed that certain surface oxides at edges and defect sites of GO might play a crucial role as the active sites in reaction with nitrogen precursors (the amino groups and the carbon nitride intermediates produced by thermal polymerization) for C−N bond formation, affording N-doping into the graphene layers, which is consistent with XPS and Raman spectra results.[33,35,36]

The N 1s peak at the binding energy of around 400 eV was observed on all the NG-600, -700, and -800, presenting 11.39, 9.68, and 8.23 at. % nitrogen doping levels, respectively. Nitrogen contents in the graphene layer would reduce at an elevated temperature due to the breakup of C−N bonds.[33,34] In this study, the catalysts had a high N-doping level (8.23−11.39 at. %), compared to those obtained from other reported methods such as the enhanced chemical vapor deposition (CVD) (5.0 at. %[37]), plasma method (5.8 at. %[32]), annealing GO with NH_3 at 300−1100 °C (3−5 at. %[33]), and with ammonium nitrate at 350 °C (5.61 at. %[21]), suggesting that the melamine could act as a novel and efficient N precursor.

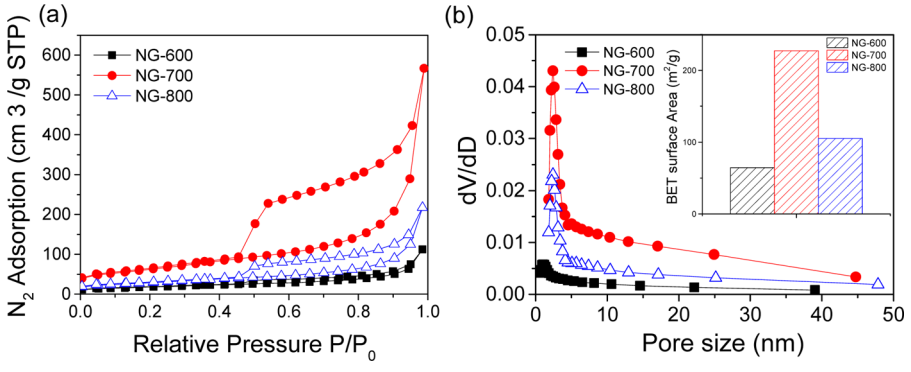

Figure 4. (a) N_2 sorption isotherms, and (b) pore size distributions and BET surface area of NG-600, -700, and -800.

DOI: 10.1021/am508416n
ACS Appl. Mater. Interfaces 2015, 7, 4169−4178

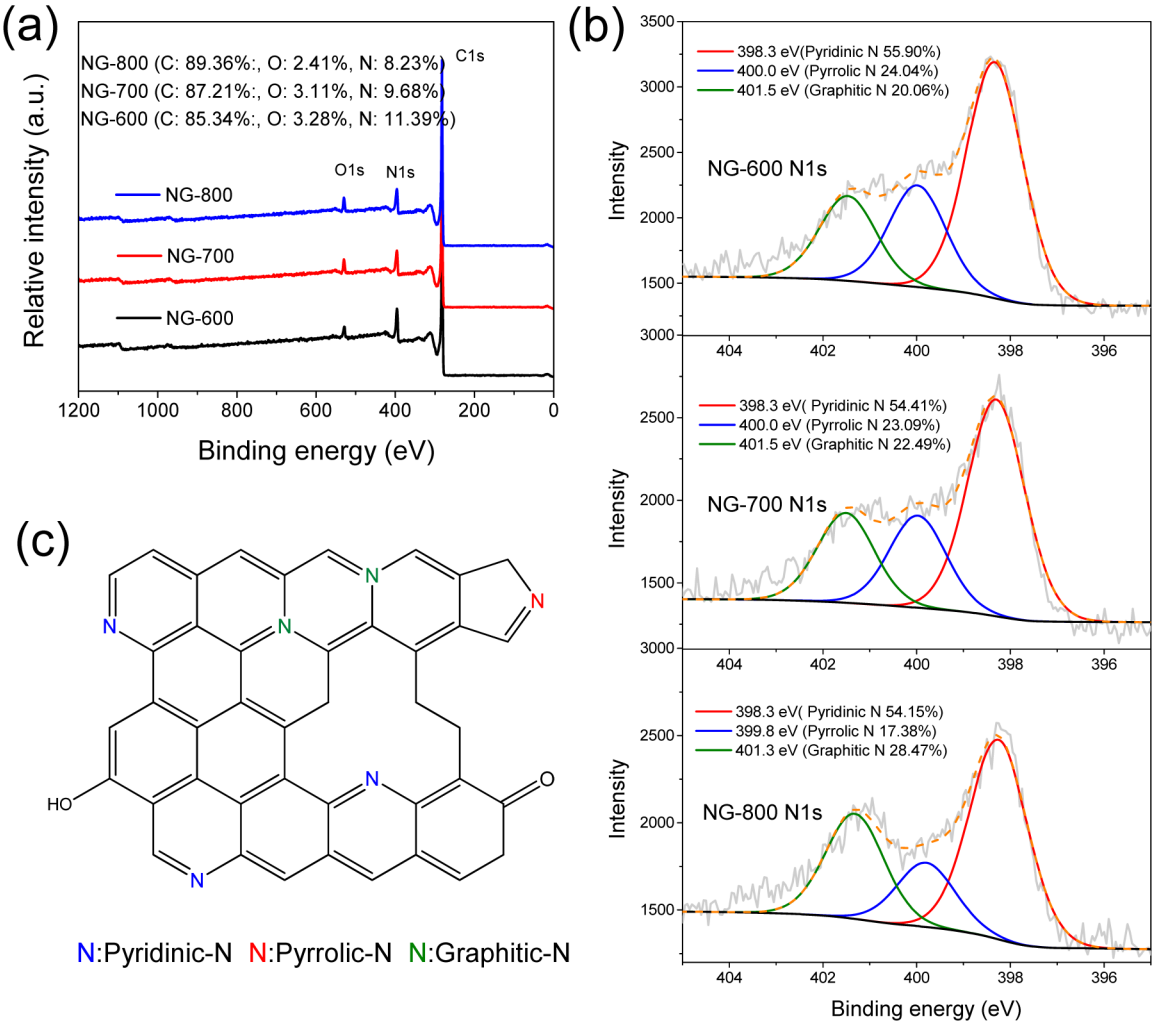

Figure 5. (a) XPS survey of NG-600, NG-700, and NG-800. (b) N 1s scan of NG-600, NG-700, and NG-800. (c) Different types of N-doping.

Figure 5b displays the high-resolution N 1s XPS spectra in a narrow range (393−407 eV). N signals were fitted into three components: 398.3, 400.0, and 401.5 eV, corresponding to pyridinic N (nitrogen in a six-atom heterocyclic ring), pyrrolic N (nitrogen in a five-atom heterocyclic ring), and quaternary N (or graphitic N, sp^2-hybridized N neighbored with three sp^2-C), respectively.[5,21,32,8] The structures of different N species are shown in Figure 5c. It can been seen that, with elevated annealing temperature from 600 to 800 °C, more graphitic N incorporated into the graphene basal plane from 20.06 to 28.47% due to the better thermal stability compared to pyrrole-like N.[33,35,39] Thus, the nitrogen compositional species and doping content could be controlled by synthesis conditions.

3.2. Catalytic Performance of Carbon Materials in Phenol Degradation. The catalytic activities of various carbocatalysts were investigated in catalytic activation of PMS for phenol oxidation in aqueous solution. Figure 6a shows that PMS itself can hardly generate active radicals for phenol degradation without a solid catalyst. Meanwhile, without the addition of PMS, only around 4% phenol was removed on NG-700 due to adsorption. Moreover, the GO and g-C_3N_4 (product from melamine polymerization) were not able to effectively activate PMS for the phenol oxidation reactions, indicating that the doped nitrogen was the active sites. Figure 6b reveals that NG-700 exhibited a greater catalytic performance to activate PMS for phenol degradation, compared to other nanocarbons such as graphene nanosheets (GNs), single-walled carbon nanotubes (SWCNTs), rGO-700, N-doped rGO, and MWCNTs using ammonium nitrate as the N precursor (NG-350 and N-CNT-350, respectively) and a typical metal catalyst, Co_3O_4. A pseudo-first-order reaction was employed to estimate the kinetic rates, as shown below:

$$\ln\left(\frac{C}{C_0}\right) = -kt \quad (1)$$

The reaction rate constants (k) of phenol oxidation on NG-700, rGO-700, GNs, SWCNTs, NG-350, N-CNT-350, and crystalline Co_3O_4 were then evaluated to be 0.319, 0.004, 0.00138, 0.00697, 0.00995, 0.00851, and 0.0173 min^{-1}, respectively. Upon nitrogen doping, the activity of rGO obtained from reduction at 700 °C with the same method can be enhanced by about 80 times. NG-700 not only showed a higher efficiency than other carbon allotropes, but superior to the popular metal-based catalyst of crystalline Co_3O_4 with more than 18 times enhancement.

Figure S4 (Supporting Information) further shows that all the samples of NG-600, -700, and -800 can completely degrade 20 ppm phenol within 15 min. In the same reaction conditions, they demonstrated much better catalytic performance than the carbon-based catalysts such as graphene (70% phenol removal

DOI: 10.1021/am508416n
ACS Appl. Mater. Interfaces 2015, 7, 4169−4178

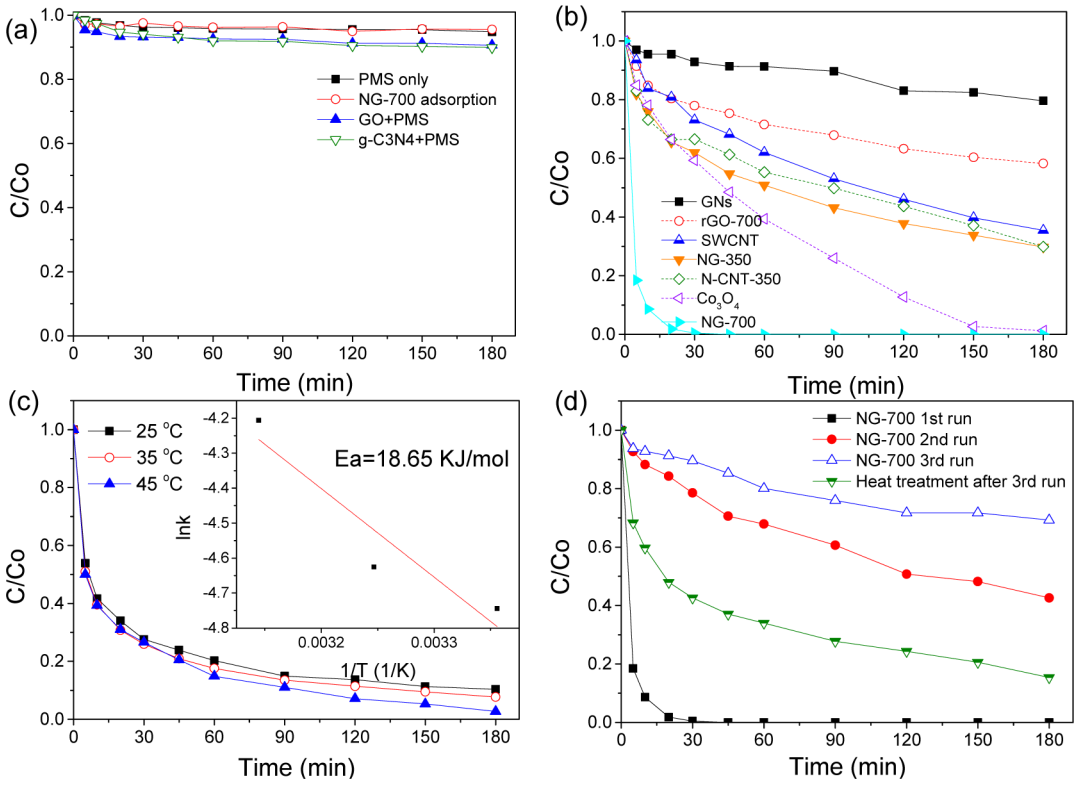

Figure 6. (a) Phenol degradation under various reaction conditions. (b) PMS activation under various catalysts. (c) Effect of temperature on phenol removal (catalyst = 0.05 g/L). (d) Stability and recyclability studies of NG-700 (catalyst, 0.1 g/L; PMS, 6.5 mM. Phenol, 20 mg/L; *T*, 25 °C).

in 180 min), N-doped graphene (annealing GO with ammonium nitrate at 350 °C), and N-modified multiwalled CNTs with complete removal of phenol in 45 min in previous studies.[14,20,21] Figure S5 (Supporting Information) shows that approximate 75% TOC removal was achieved on NG-700 in 60 min.

NG-700 shows the best performance among the NGs (Figure S4, Supporting Information), thus it was chosen for subsequent kinetic and stability studies. The influence of reaction temperature on phenol degradation is presented in Figure 6c. Interestingly, it was found that temperature presented only a marginal effect on the process of catalytic oxidation of phenol solution, which was also discovered in another study employing the N-doped carbon nanotube (N-CNT) as an effective catalyst for organic pollutant removal.[14] It suggests that the N-doping modification might lead to this effect, compared with rGO-700 without doping in Figure S6 (Supporting Information). The activation energy of NG-700 for catalytic oxidation of phenol was calculated to be 18.6 kJ/mol, lower than the reported value of CNT (33.3 kJ/mol), N-CNT (39.2 kJ/mol), and graphene (84.0 kJ/mol).[14,21] The induced N atoms could significantly activate the sp^2 carbon system and reduce the activation energy for electron transfer from graphene surface to PMS, and impose a more significant impact on the processes of PMS activation.

Figure S7 (Supporting Information) displays the effect of initial phenol concentration on its degradation rate. It was found that phenol degradation efficiency tended to drop quickly with increasing initial phenol contents in solution. It can been seen that 100% phenol was degradated in 5 and 60 min for 20 and 50 mg/L, respectively, whereas only 75% phenol was degraded in 180 min at a phenol concentration of 100 mg/L. The adsorbed phenol molecules and intermediates would cover the active sites of the catalyst, then hinder the activation of PMS. Moreover, the insufficient PMS might also be a limiting factor for degradation of high concentration of phenol solutions. Figure S8 (Supporting Information) reveals the effect of catalyst dosage on phenol removal. At 0.05 g/L, 90% of phenol removal can be achieved in 180 min, which can be significantly reduced to 30 and 5 min on a loading of 0.1 and 0.2 g/L, respectively. The increase of catalyst dosage will bring in more active sites to activate PMS, giving rise to the enhancement of catalytic efficiency.

The stability and reusability were evaluated as shown in Figure 6d. Around 58 and 31% of phenol was removed after 180 min in the second and third runs, respectively, compared to 100% decomposition of phenol in 45 min for the fresh catalyst. A thermal treatment was applied to burn the covered intermediates on the active sites and edges of the catalyst. The activity was partially recovered through the thermal annealing and 85% phenol removal was achieved, compared 31% removal at third run in 180 min. The long-term stability of the metal-free NG is not comparable to most metal catalysts, which was also reported in other heterogeneous catalytic systems.[21,40,41] As shown in Table S1 (Supporting Information) and Figure S9 (Supporting Information), the specific surface area decreased from 227.5 to 202.8 m^2/g and the pore volume reduced from 0.67 to 0.46 cm^3/g after the first run, while no apparent changes were found in average pore size. Moreover, the XPS spectra revealed a great increase of oxygen level to 13.74 at. % and a decrease of N-doping level to 1.56 at. % on the used catalysts. The deactivation of the catalyst might be ascribed to intricate influences of surface chemistry and structural changes, including the adsorption of intermediates, coverage of surface active sites, changes of pore structures, and dopants refabrication in graphene network. The activity of

DOI: 10.1021/am508416n
ACS Appl. Mater. Interfaces 2015, 7, 4169−4178

passivated catalysts could be recovered via thermal annealing (Figure 6d) or hydrogenation at a mild condition to remove the adsorbed intermediates and to create a better reductive degree of graphene. Recently, we discovered that N-doped carbon nanotubes presented a much better stability than rGO, owing to that the surface chemistry of the rolled graphene shells of CNTs was more stable and robust than the chemically derived graphene with a highly defective degree.[6] It was indicated that nitrogen doped graphene with a robust structure and a higher doping level could be more stable in metal-free catalysis.

3.3. Mechanism of Generation and Evolution of Active Radicals and Reaction Pathways. Nanocarbons have demonstrated a promising activity for PMS activation for organic pollutant removal, yet the mechanism of activation processes has not been clearly illustrated.[14,42,43] It was suggested that sp^2 carbon, zigzag edges, and electron rich-containing oxides such as carboxyl and quinone might work as the real active sites to activate PMS for the advanced oxidation processes.[14,17,18] It was further suggested that substantial modification with nitrogen can dramatically enhance the catalytic performance of rGO and MWCNTs.[20,21]

It was well reported that the introduction of heteroatoms into graphene layer would disrupt sp^2-hybridized carbon configuration and modulate the physical, chemical, and electrical properties of graphene, meanwhile create new active sites for various reactions.[4,7,44] Theoretical studies indicated that the graphitic N, with a smaller covalent radius and higher electronegativity than C atom, can induce electron transfer from adjacent carbon atoms to nitrogen, thus breaking the chemical inertness of the sp^2 carbon layer and altering the catalytic activity of graphene.[29,39,45] Luo et al.[46] demonstrated that pyridinic N, with a pair of lone electrons, is able to effectively alter the valence band of graphene and improve the π states of Fermi level. Long and co-workers[38] found that the quaternary N could be the metal-free active sites for selectively catalytic oxidation of benzylic alcohol. Both theoretical and experimental investigations have shown that the graphitic nitrogen sites may lead to high charge density and asymmetric spin density and present extraordinary electron-catalytic activity toward oxygen reduction reaction (ORR), and more active sites can then be created with the enhancing nitrogen contents.[47−50]

The proposed mechanism of PMS activation on N-doped graphene is illustrated in Scheme 3. We propose that delocalized electrons from the zigzag edges of graphene would be able to demonstrate a high chemical activity and could be transferred to activate the PMS to generate radicals.[15,51,52] The Lewis basic sites with lone electrons such as ketonic groups, pyridinic, and pyrrolic N can present an extraordinary potential for the redox process.[16] Moreover, sp^2-hybridized C in the graphene can be further activated by substantial doping of nitrogen atoms (graphitic N). In this study, a high N-doping level (8−11 at. %) and large portion of substitutional doping (graphitic N, 20−28%) were achieved by a facile one-pot doping strategy. Both characterization and experimental results indicated that the catalytic activation of N-rGO does not simply rely on the N contents, but on the structure of graphene and N species. The graphitic N might play a dominant role for PMS activation as the positively charged adjacent carbon atoms presented greater potential for the chemical adsorption of HSO_5^- and breaking the O−O bond ($HO-SO_4^-$) to generate active radicals.

Theoretical calculations were then applied to give further insights into PMS activation process on graphene and N-doped graphene in different systems as shown in Scheme 2. The minimum energy of each system was set as the basis energy when calculating the relative total energy (E_{tot}). The adsorption energy of PMS (E_b) on graphene was calculated by $E_b = E_{graphene+PMS} - E_{graphene} - E_{PMS}$, where $E_{graphene+PMS}$, $E_{graphene}$, and E_{PMS} are total energies of graphene with PMS adsorption, graphene only, and free PMS molecule, respectively. Q is the electron transfer between PMS and graphene. It was observed from Table 1 that, compared with pristine graphene (panel a), the adsorption enhancement for PMS was mainly induced by the graphitic N (panels d and e), where a higher adsorption energy was found and more electrons were transferred from graphene to PMS. For the other two types of N-doping with pyridinic N (panel b) and pyrrolic N (panel c), the changes of adsorption energy and electron transfer were not significant. Therefore, the graphitic N-doping can enhance the interaction between PMS and graphene, possibly inducing a higher activity for PMS adsorption and activation via getting electrons from graphene system and producing active radicals.

EPR spectra were acquired to experimentally probe the PMS activation processes. Figure 7a indicates that very few active radicals were generated by PMS itself without a catalyst and NG-700 presents excellent performance in PMS activation. Two types of radicals, $^{\bullet}OH$ and $SO_4^{\bullet-}$, were detected during the activation and oxidation processes. The quantitative information of DMPO−SO_4 adducts (α_H = 0.78, α_H = 1.48, α_H = 9.6, and α_N = 13.2) and DMPO−OH adducts (α_H = 14.8, α_N = 14.8) is presented in Figure 7b. The spectra are shown in Figure S10 (Supporting Information). Huang et al.[53] reported that the sulfate radicals served as the primary active species for catalytic oxidation of organic pollutants, whereas the initially produced hydroxyl radicals tended to activate PMS to produce sulfate radicals. In this study, lots of $^{\bullet}OH$ were generated in the first 1 min, then its amount quickly dropped and raised again after 5 min, and the $SO_4^{\bullet-}$ presented the same trend with relative lower amounts. It was suggested that the NGs are able to effectively activate PMS to produce sulfate and hydroxyl radicals. The rapid drop of $^{\bullet}OH$ amount was due to the consumption by phenol oxidation and the interconversion to $SO_4^{\bullet-}$ (eq 3). An upward trend after 5 min might be ascribed to the accumulation of $^{\bullet}OH$ produced from PMS and transformation of $SO_4^{\bullet-}$ (eqs 2 and 6) as most phenol molecules have been decomposed in the meantime. Sulfate radicals were consumed for oxidation of phenol and transferred to $^{\bullet}OH$ (eqs 7 and 6) during the whole reaction. The EPR results strongly proved that NG-700 can effectively activate

Scheme 3. Proposed Mechanism of PMS Activation and Phenol Oxidation on N-Doped Graphene

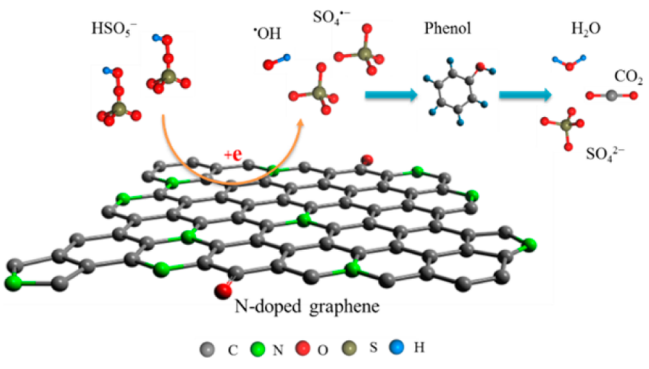

DOI: 10.1021/am508416n
ACS Appl. Mater. Interfaces 2015, 7, 4169−4178

Table 1. DFT Calculation Results for PMS Activation on Different Graphene Models

	position	E_{tot} (Ha)	E_b (eV)	Q (e)
graphene (panel a, E_{tot} = −1608.94 Ha)	1	−2383.41	−1.69	−0.556
	2	−2383.41	−1.62	−0.543
N-doped graphene (panel b, E_{tot} = −1624.97 Ha)	1	−2399.45	−1.59	−0.536
	2	−2399.45	−1.54	−0.519
	3	−2399.45	−1.54	−0.523
N-doped graphene (panel c, E_{tot} = −1586.22 Ha)	1	−2360.70	−1.81	−0.565
	2	−2360.71	−1.93	−0.438
	3	−2360.61	0.69	−0.516
N-doped graphene (panel d, E_{tot} = −1625.53 Ha)	1	−2400.04	−2.67	−0.888
	2	−2400.06	−2.98	−0.855
	3	−2400.04	−2.49	−0.767
N-doped graphene (panel e, E_{tot} = −1625.53 Ha)	1	−2400.05	−2.77	−0.831
	2	−2400.05	−2.69	−0.887
	3	−2400.04	−2.46	−0.889

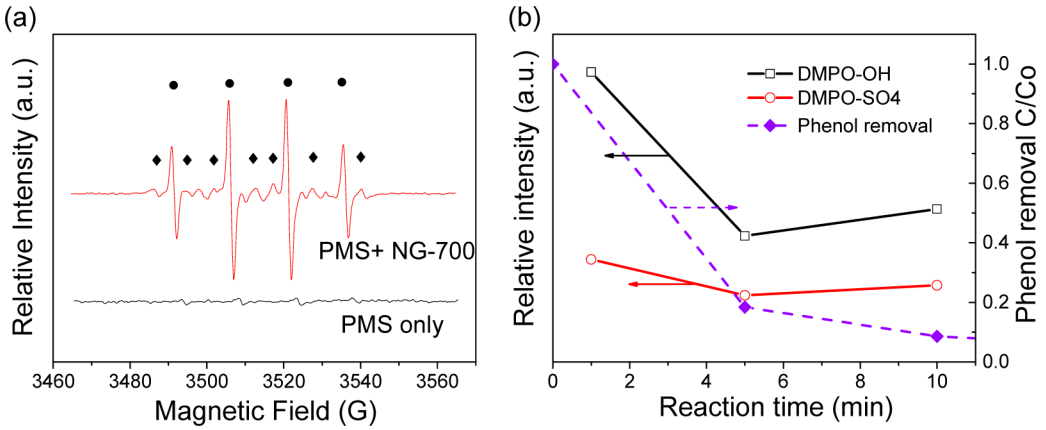

Figure 7. (a) EPR spectra of DMPO adducts under different conditions (●, DMPO−OH; ♦, DMPO−SO_4). (b) Intensity changes of DMPO adducts (Catalyst, 0.1 g/L; PMS, 6.5 mM. Phenol, 20 mg/L; *T*, 25 °C. DMPO: 0.16 mol/L).

PMS to produce sulfate and hydroxyl radicals, and large quantity of $^{\bullet}OH$ generated initially might play a crucial role for phenol degradation in the first few minutes. The competitive radical tests shown in Figure S11 (Supporting Information) suggested that sulfate radicals also played a critical role for complete decomposition of phenol. It can be deduced that both $^{\bullet}OH$ and $SO_4^{\bullet-}$ work as active radicals to attack phenol compound during the oxidation process, and the generation of $SO_4^{\bullet-}$ might have a close relationship with the initial existence of $^{\bullet}OH$ in PMS activation. Scheme S1 (Supporting Information) shows the possible degradation pathways, and the related intermediates are shown in Figures S12 and S13 (Supporting Information).

$$HSO_5^- + e^- \rightarrow {}^{\bullet}OH + SO_4^{2-} \quad (2)$$

$$HSO_5^- + e^- \rightarrow SO_4^{\bullet-} + OH^- \quad (3)$$

$$HSO_5^- - e^- \rightarrow SO_5^{\bullet-} + H^+ \quad (4)$$

$$^{\bullet}OH + SO_4^{2-} \rightarrow SO_4^{\bullet-} + OH^- \quad (5)$$

$$SO_4^{\bullet-} + OH^- \rightarrow SO_4^{2-} + {}^{\bullet}OH \quad (6)$$

$$\text{phenol} + SO_4^{\bullet-} \rightarrow \text{several steps} \rightarrow CO_2 + H_2O + SO_4^{2-} \quad (7)$$

4. CONCLUSIONS

Nitrogen-doped reduced graphene oxide with both structural and compositional modification was synthesized by a one-pot method. The prepared N-doped graphene had larger SSAs and higher nitrogen contents. N-doped graphene showed outstanding performance in catalytic activation of PMS for oxidation of phenol, and was superior to many other carbon allotropes and a typical metal-based catalyst of Co_3O_4. Kinetic studies indicated that the initial phenol concentration and catalyst dosage will influence the kinetic rate, whereas the temperature does not show a strong effect. Theoretical calculations illustrated that quaternary N is able to dramatically reduce the adsorption energy and facilitate electron transfer for PMS activation on graphene sheets. EPR spectra and competitive radical tests suggested that both $^{\bullet}OH$ and $SO_4^{\bullet-}$ were generated during the activation processes and played key roles for phenol degradation. The reaction pathways were illustrated by identification of the intermediates. This study not only provided an excellent metal-free catalyst but also, for the first time, illustrated the PMS activation and phenol degradation on nanocarbons. This metal-free catalysis will be significantly contributing to the pursuit of a sustainable remediation technology without any secondary contamination. With the development of state-of-the-art technology to synthesize low-cost and large-scale GO and graphene in the near future, this study will significantly contribute to develop-

DOI: 10.1021/am508416n
ACS Appl. Mater. Interfaces 2015, 7, 4169−4178

ment of highly robust and effective carbocatalysts for practical applications in aqueous reactions including water treatment.

■ ASSOCIATED CONTENT

Supporting Information

Preparation procedures of GO, N-rGO-350, N-CNT-350, and nanocrystalline Co_3O_4; FTIR, TGA, XPS C 1s spectra; test of intermediates, TOC, kinetic studies, and EPR spectra. The material is available free of charge via the Internet at http://pubs.acs.org.

■ AUTHOR INFORMATION

Corresponding Authors

*S. Wang. E-mail: shaobin.wang@curtin.edu.au. Phone: +61 8 9266 3776.

*H. Sun. E-mail: h.sun@curtin.edu.au. Phone: +61 8 9266 9211.

Notes

The authors declare no competing financial interest.

■ ACKNOWLEDGMENTS

We thank the Australian Research Council (ARC) for financial support under the project of DP130101319. The authors also acknowledge the Curtin University Electron Microscope Facility partially funded by the University, State, and Commonwealth Governments for providing the equipment, scientific and technical assistance. H. S. appreciates the partial support from Curtin Research Fellowship.

■ REFERENCES

(1) Geim, A. K.; Novoselov, K. S. The Rise of Graphene. *Nat. Mater.* **2007**, *6*, 183−191.

(2) Zhu, Y. W.; Murali, S.; Cai, W. W.; Li, X. S.; Suk, J. W.; Potts, J. R.; Ruoff, R. S. Graphene and Graphene Oxide: Synthesis, Properties, and Applications. *Adv. Mater.* **2010**, *22*, 3906−3924.

(3) Loh, K. P.; Bao, Q. L.; Ang, P. K.; Yang, J. X. The Chemistry of Graphene. *J. Mater. Chem.* **2010**, *20*, 2277−2289.

(4) Su, D. S.; Perathoner, S.; Centi, G. Nanocarbons for the Development of Advanced Catalysts. *Chem. Rev.* **2013**, *113*, 5782−5816.

(5) Lai, L. F.; Potts, J. R.; Zhan, D.; Wang, L.; Poh, C. K.; Tang, C. H.; Gong, H.; Shen, Z. X.; Jianyi, L. Y.; Ruoff, R. S. Exploration of the Active Center Structure of Nitrogen-Doped Graphene-based Catalysts for Oxygen Reduction Reaction. *Energy Environ. Sci.* **2012**, *5*, 7936−7942.

(6) Duan, X.; Sun, H.; Wang, Y.; Kang, J.; Wang, S. N-Doping-Induced Nonradical Reaction on Single-Walled Carbon Nanotubes for Catalytic Phenol Oxidation. *ACS Catal.* **2015**, *5*, 553−559.

(7) Su, D. S.; Zhang, J.; Frank, B.; Thomas, A.; Wang, X. C.; Paraknowitsch, J.; Schlogl, R. Metal-Free Heterogeneous Catalysis for Sustainable Chemistry. *ChemSusChem* **2010**, *3*, 169−180.

(8) Chizari, K.; Deneuve, A.; Ersen, O.; Florea, I.; Liu, Y.; Edouard, D.; Janowska, I.; Begin, D.; Cuong, P. H. Nitrogen-Doped Carbon Nanotubes as a Highly Active Metal-Free Catalyst for Selective Oxidation. *ChemSusChem* **2012**, *5*, 102−108.

(9) Anipsitakis, G. P.; Dionysiou, D. D. Degradation of Organic Contaminants in Water with Sulfate Radicals Generated by the Conjunction of Peroxymonosulfate with Cobalt. *Environ. Sci. Technol.* **2003**, *37*, 4790−4797.

(10) Anipsitakis, G. P.; Dionysiou, D. D.; Gonzalez, M. A. Cobalt-Mediated Activation of Peroxymonosulfate and Sulfate Radical Attack on Phenolic Compounds. Implications of Chloride Ions. *Environ. Sci. Technol.* **2006**, *40*, 1000−1007.

(11) Anipsitakis, G. P.; Stathatos, E.; Dionysiou, D. D. Heterogeneous Activation of Oxone Using Co_3O_4. *J. Phys. Chem. B* **2005**, *109*, 13052−13055.

(12) Liang, H. W.; Sun, H. Q.; Patel, A.; Shukla, P.; Zhu, Z. H.; Wang, S. B. Excellent Performance of Mesoporous Co_3O_4/MnO_2 Nanoparticles in Heterogeneous Activation of Peroxymonosulfate for Phenol Degradation in Aqueous Solutions. *Appl. Catal., B* **2012**, *127*, 330−335.

(13) Saputra, E.; Muhammad, S.; Sun, H. Q.; Ang, H. M.; Tade, M. O.; Wang, S. B. Different Crystallographic One-dimensional MnO_2 Nanomaterials and their Superior Performance in Catalytic Phenol Degradation. *Environ. Sci. Technol.* **2013**, *47*, 5882−5887.

(14) Sun, H. Q.; Liu, S. Z.; Zhou, G. L.; Ang, H. M.; Tade, M. O.; Wang, S. B. Reduced Graphene Oxide for Catalytic Oxidation of Aqueous Organic Pollutants. *ACS Appl. Mater. Interfaces* **2012**, *4*, 5466−5471.

(15) Enoki, T.; Fujii, S.; Takai, K. Zigzag and Armchair Edges in Graphene. *Carbon* **2012**, *50*, 3141−3145.

(16) Frank, B.; Zhang, J.; Blume, R.; Schlogl, R.; Su, D. S. Heteroatoms Increase the Selectivity in Oxidative Dehydrogenation Reactions on Nanocarbons. *Angew. Chem., Int. Ed.* **2009**, *48*, 6913−6917.

(17) Liu, S. Z.; Peng, W. C.; Sun, H. Q.; Wang, S. B. Physical and Chemical Activation of Reduced Graphene Oxide for Enhanced Adsorption and Catalytic Oxidation. *Nanoscale* **2014**, *6*, 766−771.

(18) Peng, W. C.; Liu, S. Z.; Sun, H. Q.; Yao, Y. J.; Zhi, L. J.; Wang, S. B. Synthesis of Porous Reduced Graphene Oxide as Metal-Free Carbon for Adsorption and Catalytic Oxidation of Organics in Water. *J. Mater. Chem. A* **2013**, *1*, 5854−5859.

(19) Zhang, J.; Liu, X.; Blume, R.; Zhang, A. H.; Schlogl, R.; Su, D. S. Surface-Modified Carbon Nanotubes Catalyze Oxidative Dehydrogenation of N-Butane. *Science* **2008**, *322*, 73−77.

(20) Sun, H. Q.; Kwan, C.; Suvorova, A.; Ang, H. M.; Tade, M. O.; Wang, S. B. Catalytic Oxidation of Organic Pollutants on Pristine and Surface Nitrogen-Modified Carbon Nanotubes with Sulfate Radicals. *Appl. Catal., B* **2014**, *154*, 134−141.

(21) Sun, H. Q.; Wang, Y. X.; Liu, S. Z.; Ge, L.; Wang, L.; Zhu, Z. H.; Wang, S. B. Facile Synthesis of Nitrogen Doped Reduced Graphene Oxide as a Superior Metal-Free Catalyst for Oxidation. *Chem. Commun.* **2013**, *49*, 9914−9916.

(22) Hummers, W. S.; Offeman, R. E. Preparation of Graphitic Oxide. *J. Am. Chem. Soc.* **1958**, *80*, 1339−1339.

(23) Delley, B. From Molecules to Solids with the $DMol_3$ Approach. *J. Chem. Phys.* **2000**, *113*, 7756−7764.

(24) Perdew, J. P.; Burke, K.; Ernzerhof, M. Generalized Gradient Approximation Made Simple. *Phys. Rev. Lett.* **1996**, *77*, 3865−3868.

(25) Grimme, S.; Semiempirical, G. G. A-Type Density Functional Constructed with a Long-Range Dispersion Correction. *J. Comput. Chem.* **2006**, *27*, 1787−1799.

(26) Qu, L. T.; Liu, Y.; Baek, J. B.; Dai, L. M. Nitrogen-Doped Graphene as Efficient Metal-Free Electrocatalyst for Oxygen Reduction in Fuel Cells. *ACS Nano* **2010**, *4*, 1321−1326.

(27) Su, Y. Z.; Zhang, Y.; Zhuang, X. D.; Li, S.; Wu, D. Q.; Zhang, F.; Feng, X. L. Low-Temperature Synthesis of Nitrogen/Sulfur Co-Doped Three-Dimensional Graphene Frameworks as Efficient Metal-Free Electrocatalyst for Oxygen Reduction Reaction. *Carbon* **2013**, *62*, 296−301.

(28) Ferrari, A. C.; Meyer, J. C.; Scardaci, V.; Casiraghi, C.; Lazzeri, M.; Mauri, F.; Piscanec, S.; Jiang, D.; Novoselov, K. S.; Roth, S.; Geim, A. K. Raman Spectrum of Graphene and Graphene Layers. *Phys. Rev. Lett.* **2006**, *97*, Artn: 187401.

(29) Choi, C. H.; Park, S. H.; Woo, S. I. Binary and Ternary Doping of Nitrogen, Boron, and Phosphorus into Carbon for Enhancing Electrochemical Oxygen Reduction Activity. *ACS Nano* **2012**, *6*, 7084−7091.

(30) Berciaud, S.; Ryu, S.; Brus, L. E.; Heinz, T. F. Probing the Intrinsic Properties of Exfoliated Graphene: Raman Spectroscopy of Free-Standing Monolayers. *Nano Lett.* **2009**, *9*, 346−352.

DOI: 10.1021/am508416n
ACS Appl. Mater. Interfaces 2015, 7, 4169−4178

(31) Casiraghi, C.; Pisana, S.; Novoselov, K. S.; Geim, A. K.; Ferrari, A. C. Raman Fingerprint of Charged Impurities in Graphene. *Appl. Phys. Lett.* **2007**, *91*, Artn: 233108.
(32) Kumar, N. A.; Nolan, H.; McEvoy, N.; Rezvani, E.; Doyle, R. L.; Lyons, M. E. G.; Duesberg, G. S. Plasma-Assisted Simultaneous Reduction and Nitrogen Doping of Graphene Oxide Nanosheets. *J. Mater. Chem. A* **2013**, *1*, 4431−4435.
(33) Li, X. L.; Wang, H. L.; Robinson, J. T.; Sanchez, H.; Diankov, G.; Dai, H. J. Simultaneous Nitrogen Doping and Reduction of Graphene Oxide. *J. Am. Chem. Soc.* **2009**, *131*, 15939−15944.
(34) Kinoshita, K. *Carbon: Electrochemical and Physicochemical Properties*; Wiley: New York, 1988, ISBN:978-0-471-84802-8.
(35) Sheng, Z. H.; Shao, L.; Chen, J. J.; Bao, W. J.; Wang, F. B.; Xia, X. H. Catalyst-Free Synthesis of Nitrogen-Doped Graphene via Thermal Annealing Graphite Oxide with Melamine and Its Excellent Electrocatalysis. *ACS Nano* **2011**, *5*, 4350−4358.
(36) Lin, Z. Y.; Waller, G.; Liu, Y.; Liu, M. L.; Wong, C. P. Facile Synthesis of Nitrogen-Doped Graphene via Pyrolysis of Graphene Oxide and Urea, and Its Electrocatalytic Activity toward the Oxygen-Reduction Reaction. *Adv. Energy Mater.* **2012**, *2*, 884−888.
(37) Wang, C. D.; Zhou, Y. A.; He, L. F.; Ng, T. W.; Hong, G.; Wu, Q. H.; Gao, F.; Lee, C. S.; Zhang, W. J. In Situ Nitrogen-Doped Graphene Grown from Polydimethylsiloxane by Plasma Enhanced Chemical Vapor Deposition. *Nanoscale* **2013**, *5*, 600−605.
(38) Long, J. L.; Xie, X. Q.; Xu, J.; Gu, Q.; Chen, L. M.; Wang, X. X. Nitrogen-Doped Graphene Nanosheets as Metal-Free Catalysts for Aerobic Selective Oxidation of Benzylic Alcohols. *ACS Catal.* **2012**, *2*, 622−631.
(39) Deng, D. H.; Pan, X. L.; Yu, L. A.; Cui, Y.; Jiang, Y. P.; Qi, J.; Li, W. X.; Fu, Q. A.; Ma, X. C.; Xue, Q. K.; Sun, G. Q.; Bao, X. H. Toward N-Doped Graphene via Solvothermal Synthesis. *Chem. Mater.* **2011**, *23*, 1188−1193.
(40) Kong, X. K.; Sun, Z. Y.; Chen, M.; Chen, C. L.; Chen, Q. W. Metal-Free Catalytic Reduction of 4-Nitrophenol to 4-Aminophenol by N-Doped Graphene. *Energy Environ. Sci.* **2013**, *6*, 3260−3266.
(41) Kong, X. K.; Chen, C. L.; Chen, Q. W. Doped Graphene for Metal-Free Catalysis. *Chem. Soc. Rev.* **2014**, *43*, 2841−2857.
(42) Saputra, E.; Muhammad, S.; Sun, H. Q.; Wang, S. B. Activated Carbons as Green and Effective Catalysts for Generation of Reactive Radicals in Degradation of Aqueous Phenol. *RSC Adv.* **2013**, *3*, 21905−21910.
(43) Wang, S. B.; Sun, H. Q.; Ang, H. M.; Tade, M. O. Adsorptive Remediation of Environmental Pollutants Using Novel Graphene-based Nanomaterials. *Chem. Eng. J.* **2013**, *226*, 336−347.
(44) Liu, H. T.; Liu, Y. Q.; Zhu, D. B. Chemical Doping of Graphene. *J. Mater. Chem.* **2011**, *21*, 3335−3345.
(45) Gong, K. P.; Du, F.; Xia, Z. H.; Durstock, M.; Dai, L. M. Nitrogen-Doped Carbon Nanotube Arrays with High Electrocatalytic Activity for Oxygen Reduction. *Science* **2009**, *323*, 760−764.
(46) Luo, Z. Q.; Lim, S. H.; Tian, Z. Q.; Shang, J. Z.; Lai, L. F.; MacDonald, B.; Fu, C.; Shen, Z. X.; Yu, T.; Lin, J. Y. Pyridinic N Doped Graphene: Synthesis, Electronic Structure, and Electrocatalytic Property. *J. Mater. Chem.* **2011**, *21*, 8038−8044.
(47) Lu, Z. J.; Bao, S. J.; Gou, Y. T.; Cai, C. J.; Ji, C. C.; Xu, M. W.; Song, J.; Wang, R. Y. Nitrogen-Doped Reduced-Graphene Oxide as an Efficient Metal-Free Electrocatalyst for Oxygen Reduction in Fuel Cells. *RSC Adv.* **2013**, *3*, 3990−3995.
(48) Geng, D. S.; Chen, Y.; Chen, Y. G.; Li, Y. L.; Li, R. Y.; Sun, X. L.; Ye, S. Y.; Knights, S. High Oxygen-Reduction Activity and Durability of Nitrogen-Doped Graphene. *Energy Environ. Sci.* **2011**, *4*, 760−764.
(49) Nagaiah, T. C.; Kundu, S.; Bron, M.; Muhler, M.; Schuhmann, W. Nitrogen-Doped Carbon Nanotubes as a Cathode Catalyst for the Oxygen Reduction Reaction in Alkaline Medium. *Electrochem. Commun.* **2010**, *12*, 338−341.
(50) Zhang, L. P.; Niu, J. B.; Li, M. T.; Xia, Z. H. Catalytic Mechanisms of Sulfur-Doped Graphene as Efficient Oxygen Reduction Reaction Catalysts for Fuel Cells. *J. Phys. Chem. C* **2014**, *118*, 3545−3553.
(51) Lee, G.; Cho, K. Electronic Structures of Zigzag Graphene Nanoribbons with Edge Hydrogenation and Oxidation. *Phys. Rev. B* **2009**, *79*, Artn: 165440.
(52) Jiang, D. E.; Sumpter, B. G.; Dai, S. Unique Chemical Reactivity of a Graphene Nanoribbon's Zigzag Edge. *J. Chem. Phys.* **2007**, *126*, Artn: 134701.
(53) Huang, Z. F.; Bao, H. W.; Yao, Y. Y.; Lu, W. Y.; Chen, W. X. Novel Green Activation Processes and Mechanism of Peroxymonosulfate Based on Supported Cobalt Phthalocyanine Catalyst. *Appl. Catal., B* **2014**, *154*, 36−43.

DOI: 10.1021/am508416n
ACS Appl. Mater. Interfaces 2015, 7, 4169−4178